IJNRD.ORG ISSN : 2456-4184
INTERNATIONAL JOURNAL OF NOVEL RESEARCH AND DEVELOPMENT (IJNRD) | IJNRD.ORG
An International Open Access, Peer-reviewed, Refereed Journal

MODELLING AND SIMULATION OF A ROBOTIC GARRI FRYER KINEMATICS

[1] Matthew O. Akusu, [2] Kaiser I. Amuche
[12]Senior officer,
[12]Department of Electrical and Electronics Engineering,
[12] Petroleum Training Institute, Effurun, Nigeria.

Abstract : This paper presents the modelling and simulation of a 2-degree of freedom garri frying robotic arm. The robotic arm was developed to curtail the hazards faced by local farmers such as burns and injuries commonly associated with garri processing. The garri turner automatically moves to the center of the frying bowl via inverse kinematics solved using particle swarm optimisation. Thereafter, the garri turner is made to rotate both clockwise and counterclockwise using a 24 V sinusoidal reference signal with a 1.25 rad/s frequency while simultaneously controlling the temperature of the garri frying bowl at 100 and 200 degrees Celsius to achieve the garri frying process efficiently.

IndexTerms - **Robotics, Food Processing, Garri,Garri Processing**

I. INTRODUCTION

The advent of technology has come to ease the burden of man with the application of machines that can perform human tasks faster, easier, and more optimal than man (Onu, 2020). Modern technology has been applied in the production and processing of pounded yam, fried garri, pounded cassava flour, grains grindings, rice milling, and so on (Miriam, 2017, Onokwai et al., 2019, Nwadinobi et al., 2019,and Onu, 2020). However, this paper is limited to the application of modern technology in the frying of garri.
Garri is a product of processed fermented mashed cassava tuber and it is consumed by several millions of people in the West African sub-region and Some parts of Brazil in particular regardless of ethnicity and socio-economic class. However, production and handling methods have not been standardized resulting in a product with varying quality and safety indices hence varying public health concerns (Aturamu et al., 2021, Thomas et al., 2021). Garri which can also be called granulated Cassava or Cassava Granules is a product of processed Cassava. It is mainly a creamy white granular flour with a slightly fermented flavor and sour taste made from fermented gelatinized fresh Cassava Tubers (Isitor et al., 2019, Onokwai et al., 2019 and Kayode et al., 2021).

Garri processing involves a series of critical processes which includes frying as the most critical unit operation in the processing of cassava into garri (Salman et al., 2022). It is also a combination of simultaneous cooking and drying processes (Ndife, 2019). Though a dehydrating process, garri frying is not a straightforward drying process. The product is first cooked with the moisture in it and then dehydrated (Nwadinobi et al., 2019). The heat intensity during frying affects the quality of the product (Isitor et al., 2019, Nwadinobi et al., 2019 and Dike et al., 2022). The moisture content of dewatered and sieved cassava mash is between 50 to 65% which has to be reduced to 12% after the frying operation (Oloyede et al., n.d., Onu, 2020). At the end of the frying operation, the product is still hot and a little bit damp, it is then left to cool and dry in a cool dry shade until the moisture content is reduced to 12%. In villages, garri is fried in shallow iron pans, or the more traditional areas in earthenware pans, over an open wood fire (Miriam, 2017, Abasilim et al., 2019, Gervase Ikechukwu & Paulina Chikaodili, 2020, Samuel et al., 2021 and Ezemba et al., 2022).

To limit the hazard of garri frying the process can be handled by robots which are machines that can perform complicated series of tasks automatically (Krishnaraj Rao et al., 2022). They are also useful in tasks that could be considered hazardous to humans (Çetin et al., 2021). Robotics is an interdisciplinary branch of Engineering and Science, which includes; Mechanical Engineering, Electrical Engineering, Computer Science, etc (Dawoud et al, 2019). The term robotics deals with the Design, Construction, Operation, and Usage. The computer system used in robotics is for their control, sensory feedback, and information processing. They are used in different fields such as industry, military, space exploration, medical applications, and so on (Tsai et al., 2020, Pradhan et al., 2021 and Ali et al., 2022). In the manufacturing industry, one of the most used robots is the robotic arm. They are usually made up of 2 to 6 joints and can be used for several manufacturing applications such as welding, material handling, and removal. The robot arm closely resembles a human arm, with a wrist, forearm, elbow, and shoulder. A six-axis robot arm has six degrees of freedom, which allows it to move in six different ways simultaneously.

This paper provides a 2 DoF garri frying robotic solution to curtail the hazards related to the traditional method of garri frying currently embraced by peasant farmers as it will bring about a more efficient production due to its indefatigable nature and accurate stirring ability thereby resulting in a faster production rate which meets local demand and for exportation to foreign lands. Also, a standard temperature and humidity threshold/set-point will be adopted and put in place to ensure better and more uniform/homogeneous output after frying is done.

II. METHODOLOGY

2.1 Robot Kinematics

Kinematics of a robotic manipulator involves analyses to determine the position and orientation of the end effector, relative to the base frame. This process is known as the forward kinematics. Also, it involves the calculation of all possible joint angle sets that could be used to obtain the given position and orientation of the end effector. In this case, the process is known as inverse kinematics of the manipulator (Khan, 2021).

2.2 Forward Kinematics

The Denvit-Hartenberg (DH) parameters are used to derive the homogeneous transformation matrices that facilitate the forward kinematic analysis. For a two-degree of freedom (2-DOF) robot, the DH parameters are computed based on Table 2.1 while Figure 2.1, shows a free-body diagram of the robot with 2-DOF.

Table 2.1 DH Parameters for the 2-DOF Robot

Link	a_i	α_i	d_i	θ_i
1	L_1	0	0	θ_1
2	L_2	0	0	θ_2

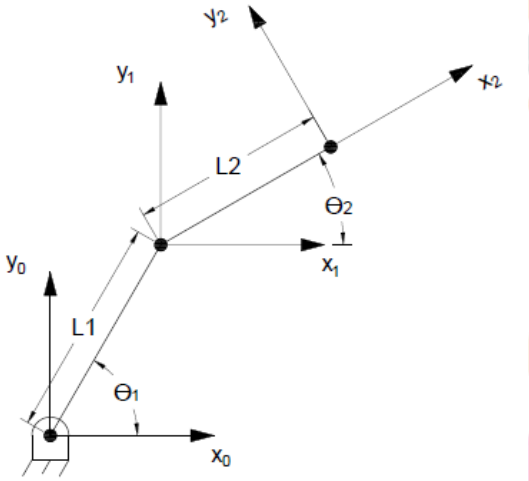

Figure 2.1 Free-body diagram of the 2 DOF Robot

In Figure 2.1, L_1, θ_1 are the length and inclination angle of the first link. Similarly, L_2, θ_2 are the length and inclination angle of the second link. The homogeneous transformation matrices for the robotic arm are derived as follows:

$$ {}^{0}_{1}\mathrm{T} = \begin{bmatrix} \cos\theta_1 & -\sin\theta_1 & 0 & L_1\cos\theta_1 \\ \sin\theta_1 & \cos\theta_1 & 0 & L_1\sin\theta_1 \\ 0 & 0 & 1 & 0 \\ 0 & 0 & 0 & 1 \end{bmatrix} \quad (2.1) $$

$$ {}^{1}_{2}\mathrm{T} = \begin{bmatrix} \cos\theta_2 & -\sin\theta_2 & 0 & L_2\cos\theta_2 \\ \sin\theta_2 & \cos\theta_2 & 0 & L_2\sin\theta_2 \\ 0 & 0 & 1 & 0 \\ 0 & 0 & 0 & 1 \end{bmatrix} \quad (2.2) $$

Adding equations (1) and (2), the homogeneous transformation matrix ${}^{0}_{2}\mathrm{T}$ now becomes:

$$ {}^{0}_{2}\mathrm{T} = \begin{bmatrix} \cos(\theta_1+\theta_2) & -\sin(\theta_1+\theta_2) & 0 & L_1\cos\theta_1 + L_2\cos(\theta_1+\theta_2) \\ \sin(\theta_1+\theta_2) & \cos(\theta_1+\theta_2) & 0 & L_1\sin\theta_1 + L_2\sin(\theta_1+\theta_2) \\ 0 & 0 & 1 & 0 \\ 0 & 0 & 0 & 1 \end{bmatrix} \quad (2.3) $$

The first three rows and columns of the transformation matrix in Equation (3) define the orientation of the fryer paddle. Thus,

$$ {}^{R}_{H}T = \begin{bmatrix} nx & ox & ax & px \\ ny & oy & ay & py \\ nz & oz & az & pz \\ 0 & 0 & 0 & 1 \end{bmatrix} \quad (2.4) $$

$$ {}^{0}_{2}T = {}^{R}_{H}T \quad (2.5) $$

From Equation (2.5), the x and y coordinates of the fryer paddle are given by Equations (2.6) and (2.7).

$$ p_x = L_1 \cos\theta_1 + L_2 \cos(\theta_1 + \theta_2) \quad (2.6) $$

$$ p_y = L_1 \sin\theta_1 + L_2 \sin(\theta_1 + \theta_2) \quad (2.7) $$

2.3 Inverse Kinematics

2.3.1 Inverse Kinematics via Geometrical Analysis

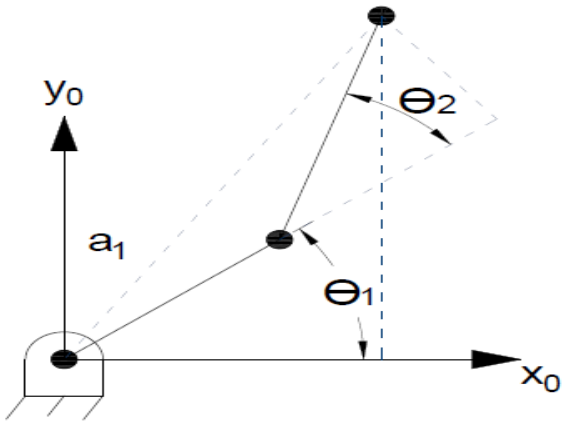

Figure 2.2 Inverse Kinematic Representation of the 2-DOF robot

Inverse kinematics involve using a particular coordinate of the end effector to determine the joint arm variables via geometrical analysis suitable for manual tuning. The geometrical method of analysis was adopted in this design. Referring to Equation (2.2), the joint angle at the elbow can be calculated by using Pythagoras theorem.

$$ \Leftrightarrow {p_x}^2 + {p_y}^2 = {L_1}^2 + {L_2}^2 + 2L_1L_2\cos\theta_2 \quad (2.8) $$

$$ \cos\theta_2 = \frac{1}{2L_1L_2}\left({p_x}^2 + {p_y}^2 - {L_1}^2 - {L_1}^2\right) \quad (2.9) $$

$$ \sin\theta_2 = \pm\sqrt{1 - \cos{\theta_2}^2} $$

$$ \text{Thus, } \theta_2 = \pm\tan^{-1}\frac{\sin\theta_2}{\cos\theta_2} \quad (2.10) $$

Also, for the joint variable, θ_1,

$$ p_x = (L_1 + L_2\cos\theta_2)\cos\theta_1 - L_2\sin\theta_2\sin\theta_2 \quad (2.11) $$

$$ p_y = L_2\sin\theta_2\cos\theta_1 + (L_1 + L_2\cos\theta_2)\sin\theta_1 \quad (2.12) $$

$$ \Delta = \begin{bmatrix} L_1 + L_2\cos\theta_2 & -L_2\sin\theta_2 \\ L_2\sin\theta_2 & L_1 + L_2\cos\theta_2 \end{bmatrix} \quad (2.13) $$

$$ {p_x}^2 + {p_x}^2 = (L_1 + L_2\cos\theta_2)^2 + (L_2\sin\theta_2)^2 \quad (2.14) $$

$$ \Delta\sin\theta_1 = \begin{bmatrix} L_1 + L_2\cos\theta_2 & p_x \\ L_2\sin\theta_2 & p_y \end{bmatrix} \quad (2.15) $$

$$ \Delta\cos\theta_1 = \begin{bmatrix} p_x & -L_2\sin\theta_2 \\ p_y & L_1 + L_2\cos\theta_2 \end{bmatrix} \quad (2.16) $$

$$ \sin\theta_1 = \frac{\Delta\sin\theta_1}{\Delta} = \frac{(L_1+L_2\cos\theta_2)p_y - L_2\sin\theta_2 p_x}{{p_x}^2+{p_y}^2} \quad (2.17) $$

$$ \cos\theta_1 = \frac{\Delta\cos\theta_1}{\Delta} = \frac{(L_1+L_2\cos\theta_2)p_x - L_2\sin\theta_2 p_y}{{p_x}^2+{p_y}^2} \quad (2.18) $$

$$ \therefore \theta_1 = \tan^{-1}\frac{\sin\theta_1}{\cos\theta_1} = \tan^{-1}\frac{(L_1+L_2\cos\theta_2)p_y \pm L_2\sin\theta_2 p_x}{(L_1+L_2\cos\theta_2)p_x \pm L_2\sin\theta_2 p_y} \quad (2.19) $$

By Euler-Lagrange method of analyzing robot dynamics was applied. It involves computing the kinetic (K_E) and potential (P_E) energies on the fryer arm to determine the Lagrangian ($\mathcal{L}$) of the system. This will facilitate computing the forces and torque applied to each joint. The Langrangian equation is given in Equation (20).

$$ \mathcal{L}\big(q(t), \dot{q}(t)\big) = K_E\big(q(t), \dot{q}(t)\big) - P_E\big(q(t)\big) \quad (2.20) $$

$$ \text{But, } P_E = mgl \quad (2.21) $$

Where m is the mass of the link (in kg),
g is the acceleration due to gravity (9.81 m/s^2)
and l is the length of the link.

$$ \text{Also, } K_E = \frac{1}{2}m\dot{x}^2 \quad (2.22) $$

Where $\dot{x}$ is the velocity; determined based on the link position with respect to time. The position of the fryer paddle is determined using the following variables:

$$x_1 = L_1 \sin\theta_1 \quad (2.24)$$

$$y_1 = L_1 \cos\theta_1 \quad (2.25)$$

$$x_2 = L_1 \sin\theta_1 + L_2 \sin(\theta_1 + \theta_2) \quad (2.26)$$

$$y_2 = L_1 \cos\theta_1 + L_2 \cos(\theta_1 + \theta_2) \quad (2.27)$$

Substituting the position variables into Equation 22,

$$K_E = \frac{1}{2} m_1 \dot{x}_1^{\,2} + \frac{1}{2} m_1 \dot{y}_1^{\,2} + \frac{1}{2} m_2 \dot{x}_2^{\,2} + \frac{1}{2} m_2 \dot{y}_2^{\,2} \quad (2.28)$$

$$K_E = \frac{1}{2}(m_1 + m_2) l_1^{\,2} \dot{\theta}_1^{\,2} + \frac{1}{2} m_2 l_1^{\,2} \dot{\theta}_1^{\,2} + \frac{1}{2} m_2 l_2^{\,2} \dot{\theta}_1 \dot{\theta}_2 + \frac{1}{2} m_2 l_2^{\,2} \dot{\theta}_2^{\,2} + m_2 l_1 l_2 \cos\theta_2 \left(\dot{\theta}_1 \dot{\theta}_2 + \dot{\theta}_1^{\,2}\right) \quad (2.29)$$

Also, the potential energy equation is given as:

$$P_E = m_1 g l_1 \cos\theta_1 + m_2 g (l_1 \cos\theta_1 + l_2 \cos(\theta_1 + \theta_2)) \quad (2.30)$$

But, the Euler-Lagrange equation is given as:

$$F = \frac{d}{dt}\left[\frac{\partial \mathcal{L}}{\partial \dot{\theta}}\right] - \frac{\partial \mathcal{L}}{\partial \theta} \quad (2.31)$$

Substituting Equations 29 and 30 into Equation 31, the Lagrangian equation is formed.

$$\mathcal{L} = \frac{1}{2}(m_1 + m_2) l_1^{\,2} \dot{\theta}_1^{\,2} + \frac{1}{2} m_2 l_1^{\,2} \dot{\theta}_1^{\,2} + \frac{1}{2} m_2 l_2^{\,2} \dot{\theta}_1 \dot{\theta}_2 + \frac{1}{2} m_2 l_2^{\,2} \dot{\theta}_2^{\,2} + m_2 l_1 l_2 \cos\theta_2 \left(\dot{\theta}_1 \dot{\theta}_2 + \dot{\theta}_1^{\,2}\right) - m_1 g l_1 \cos\theta_1 + m_2 g (l_1 \cos\theta_1 + l_2 \cos(\theta_1 + \theta_2)) \quad (32)$$

Using Equation (32), the force applied to the robot is computed with respect to Equation (31).

Thus, $F_{\theta_{1,2}} = \frac{d}{dt}\left[\frac{\partial \mathcal{L}}{\partial \dot{\theta}_{1,2}}\right] - \frac{\partial \mathcal{L}}{\partial \theta_{1,2}}$

For the first joint, the force is computed as follows:

$$F_{\theta_1} = \left((m_1 + m_2) l_1^{\,2} + m_2 l_2^{\,2} + 2 m_2 l_1 l_2 \cos\theta_2\right) \ddot{\theta}_1 + \left(m_2 l_2^{\,2} - m_2 l_1 l_2 \cos\theta_2\right) \ddot{\theta}_2 - m_2 l_1 l_2 \sin\theta_2 \left(2\dot{\theta}_1 \dot{\theta}_2 + \dot{\theta}_2^{\,2}\right) - (m_1 + m_2) l_1 g \sin\theta_1 - m_2 l_2 g \sin(\theta_1 + \theta_2) \quad (33)$$

Also, for the second joint, the force applied is given by:

$$F_{\theta_2} = \left(m_2 l_2^{\,2} + m_2 l_1 l_2 \cos\theta_2\right) \ddot{\theta}_1 + m_2 l_2^{\,2} \ddot{\theta}_2 - m_2 l_1 l_2 \sin(\theta_2) \dot{\theta}_1 \dot{\theta}_2 - m_2 l_2 g \sin(\theta_1 + \theta_2) \quad (2.34)$$

Thus, the motion of the robotic system is given by the nonlinear equation:

$$F = B(\ddot{q}) + C(\dot{q}, q) + g(q) \quad (2.35)$$

Where:

$$F = \begin{bmatrix} F_{\theta_1} \\ F_{\theta_2} \end{bmatrix} \quad (2.36)$$

$$B(\ddot{q}) = \begin{bmatrix} \left((m_1 + m_2) l_1^{\,2} + m_2 l_2^{\,2} + 2 m_2 l_1 l_2 \cos\theta_2\right) & \left(m_2 l_2^{\,2} - m_2 l_1 l_2 \cos\theta_2\right) \\ \left(m_2 l_2^{\,2} - m_2 l_1 l_2 \cos\theta_2\right) & m_2 l_2 \end{bmatrix} \quad (2.37)$$

$$C(\dot{q}, q) = \begin{bmatrix} -m_2 l_1 l_2 \sin\theta_2 \left(2\dot{\theta}_1 \dot{\theta}_2 + \dot{\theta}_2^{\,2}\right) \\ -m_2 l_1 l_2 \sin(\theta_2) \dot{\theta}_1 \dot{\theta}_2 \end{bmatrix} \quad (2.38)$$

$$g(q) = \begin{bmatrix} -(m_1 + m_2) l_1 g \sin\theta_1 - m_2 l_2 g \sin(\theta_1 + \theta_2) \\ -m_2 l_2 g \sin(\theta_1 + \theta_2) \end{bmatrix} \quad (2.39)$$

$$q = \begin{bmatrix} \theta_1 \\ \theta_1 \end{bmatrix} \quad (2.40)$$

2.3.2 Inverse Kinematics with Particle Swarm Optimisation

The particle swarm optimization (PSO) algorithm is a non-gradient optimizer that mimics the activity of particles feasting in a search space. The PSO algorithm uses random initialised particles which pose both random speed and position. Each particle can adjust the pattern of movement (p_b) with knowledge gained via exploration and in conjunction with the position of other particles while moving close to the particle with the best position (g_b) evaluated by a fitness function (Abou Omar et al. 2013, Mohanty et al. 2014). The adjustment of both the location and speed of a particle is governed mathematically as follows:

$$s_{k,l}^{(t+1)} = t * [s_{i,l}^{(t)} + c_1 r_1 * (P_{b_k} - p_{k,l}^{(t)}) + c_2 r_2 * (g_{b_k} - p_{k,l}^{(k)})] \quad (2.41)$$

$$p_{k,l}^{(t+1)} = p_{k,l}^{(t)} + v_{k,l}^{(t+1)} \quad (2.42)$$

Where, $s_{i,g}^{(t+1)}$ is particle k's speed in g- dimension at iteration $t + 1$ and $p_{k,g}^{(t+1)}$ represents the particle's location k in dimension g at iteration $t + 1$, while c_1 and c_2 respectively are cognitive and social acceleration values (Abou Omar et al. 2013, Mohanty et al. 2014).

Also, a constriction factor cn is given as follows:

$$cn = \frac{2}{\left|2 - a\sqrt{a^2 - 4a}\right|} \quad (2.43)$$

Where, $a = c_1 + c_2, a > 4$

The garri fryer robotic arm model in Simulink is shown in Figure 2.3 and the internal architecture is shown in Figure 2.4.

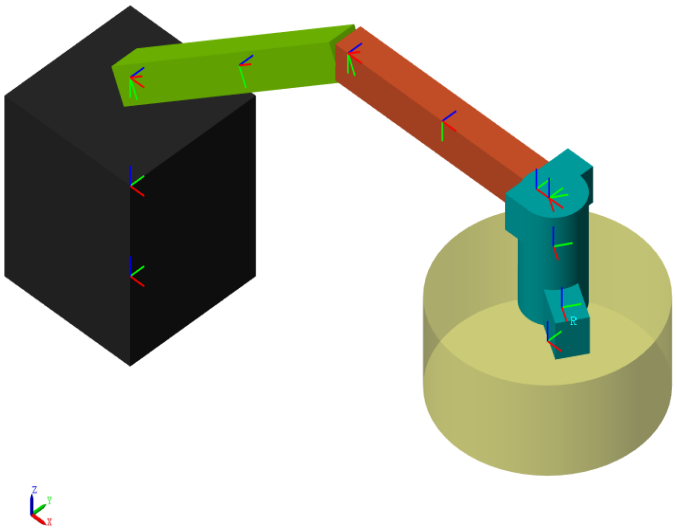

Figure 2.3 Simulink Model for the Robotic Garri Fryer

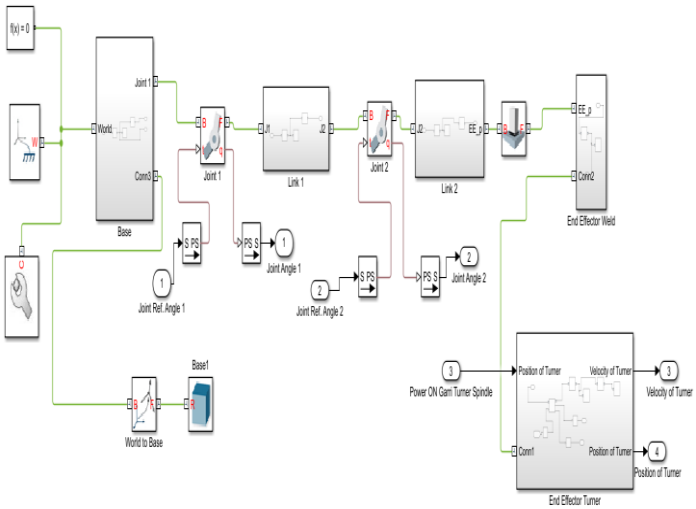

Figure 2.4 Simulink Internal Architecture of the Robotic Fryer

III. SIMULATION RESULT

The operation of the Garri frying robot using the inverse kinematics is such that, at initialization, the garri turner's end effector is in the default position [X, Y, Z] at [0.241, -0.122, 0.11]. Therefore, the end effector will only begin rotation, if placed at the center of the frying bowl, while the heating element in the bowl is simultaneously activated to heat up to a temperature of 100 ℃ for 50 seconds and 200 ℃ for another 50 seconds before the frying process is completed.

To automatically track the bowl's center point, the Robot must be able to calibrate the end effector's position from any initial position such as from coordinate [X, Y, Z] = [0.241, -0.122, 0.11], to the center of the frying pan/basin. Hence, both manual and particle swarm optimisation PSO adjustments to joint angles 1 and 2 were performed. The accuracy of the methods was compared using the mean squared error (MSE) score as shown in Table 3.1. The PSO had a low fitness score which is comparable to the manually adjusted robot joint angles.

Table 3.1 Inverse Kinematics comparing PSO and manual adjustments of the Joint angles

Inverse Kinematics Method	**Joint Angle 1 (rad)**	**Joint Angle 2 (rad)**	**X (m)**	**Y (m)**	**Z (m)**	**MSE Score**
Manual	-0.52	0.54	0.32	-0.1	0.11	0
PSO	-0.52	0.54	0.32	-0.1	0.11	2.3e-03

As shown in Figure 3.1, the angular velocity (rads/s) of the end effector is zero at initialization and remained so for 5 seconds, until the end effector moved from the default position to the center of the frying bowl. This was followed by a sinusoidal input voltage of 24V with a frequency of 1.25 rads/s applied to the garri turner motor at the end effector. Consequently, the angular velocity of the end effector oscillated between +/-3200 rads/sec at a steady state between 20 seconds and 100 seconds during the frying process. Further, the heating element in the robot bowl is deactivated at 100s since the process is presumed to have been completed. Figure 3.2, shows the temperature change in the Bowl while Figure 3.3, shows the Simulink block diagram of the robotic Garri Fryer.

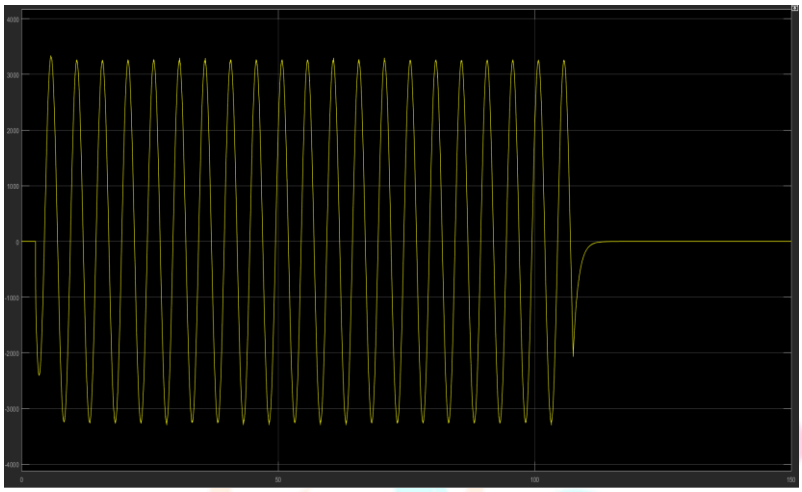

Figure 3.1 Angular Velocity (in Radians/second) of the Robotic Garri Turner's end Effector

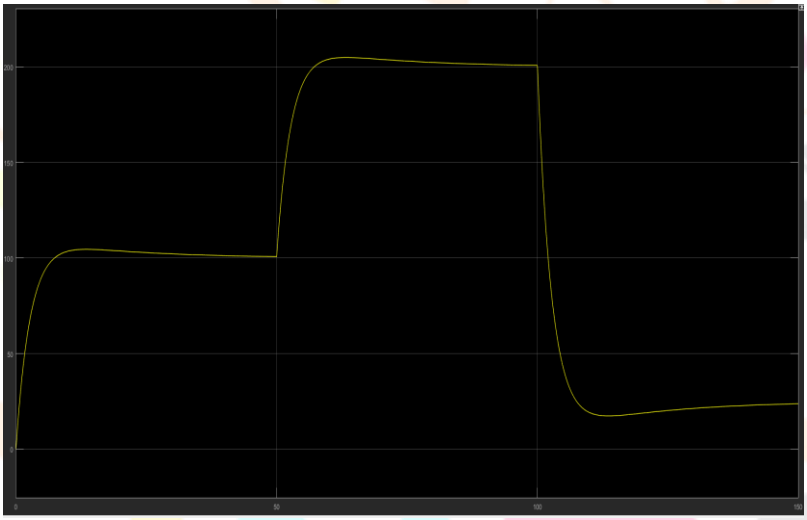

Figure 3.2 Temperature of the heated frying Bowl.

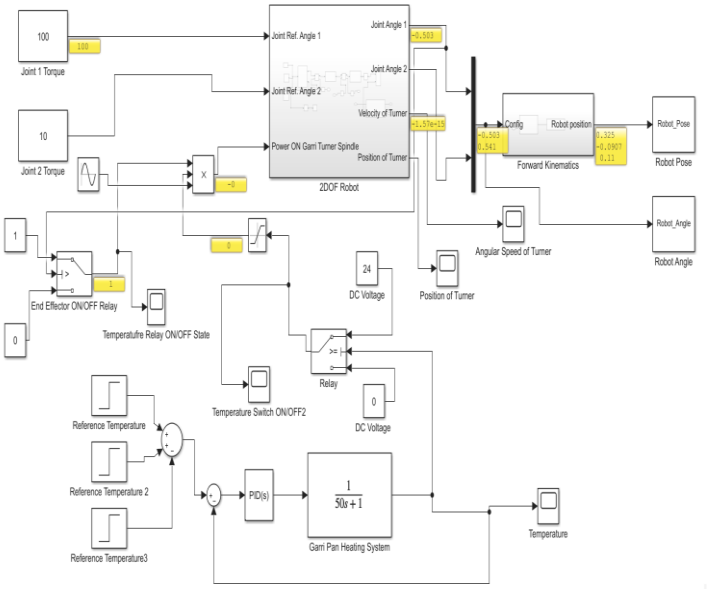

Figure 3.3 Simulink diagram of the Garri Frying robot

IV. CONCLUSION

This paper presented a 2-DoF robotic arm for frying garri efficiently while eliminating potential hazards that are faced by local farmers/indigenes during the processing. By solving the inverse kinematics between the base of the robotic arm and its end effector (garri turner), the garri turner was placed at the center of the frying bowl using both manual and automatic. The inverse kinematics via PSO was only negligibly less accurate than the manually tuned joint angle. The PID controllers which controlled the temperature of the bowl were auto-tuned in MATLAB. The overall process of garri frying was shown to be successful via the simulation results.

REFERENCES

[1] Ali, H. M., Hashim, Y., & Al-Sakkal, G. A. (2022). Design and implementation of Arduino based robotic arm. International Journal of Electrical and Computer Engineering, 12(2), 1411–1418.

[2] Aturamu, O. A., Akinbola, A. E., Omosehin, O. O., & Oguntuase, D. T. (2021). Analysis of Profitability and Market Outlets of Smallholder Garri Producers in Ondo State, Nigeria. Asian Journal of Economics, Business and Accounting, 21(1), 82–91.

[3] Dike, K. S., Okafor, C. P., Ohabughiro, B. N., Maduwuba, M. C., Ezeokoli, O. T., Ayeni, K. I., Okafor, C. M., & Ezekiel, C. N. (2022). Analysis of bacterial communities of three cassava-based traditionally fermented Nigerian foods (abacha, fufu and garri). Letters in Applied Microbiology, 74(3), 452–461.

[4] Ezemba, C. C., Ezemba, A. S., Ezemba, C. C., Igwe, K. I., Kehinde, S. O., Ezemba, S., & Okagbue, R. N. (2022). OCCURRENCE OF AMYLASE PRODUCING ORGANISMS IN CASSAVA FERMENTATION FOR GARRI PRODUCTION.

[5] Kayode, *, Adebayo, A. O., Awoyemi, S. A., & Oyeniran, A. O. (2021). Utilization of Garri-Processing Methods among Rural Women in Iwo Local Government Area, Osun State, Nigeria. JAFE, 8(2), 1–10. https://uilspace.unilorin.edu.ng/handle/20.500.12484/7375

[6] Khan, A. T. (2021). Obstacle avoidance and model-free tracking control for home automation using bio-inspired approach. Wiley Online Library, November 2020, 1–14. https://onlinelibrary.wiley.com/doi/abs/10.1002/adc2.63

[7] Krishnaraj Rao, N. S., Avinash, N. J., Rama Moorthy, H., Karthik, K., Rao, S., & Santosh, S. (2022). An Automated Robotic Arm: A Machine Learning Approach. Ieeexplore.Ieee.Org, 1–6. https://doi.org/10.1109/icmnwc52512.2021.9688512

[8] Miriam, N. M. (2017). Improved production technologies and cultural practices used by cassava producers in Enugu State, Nigeria. Idosr.Org, 2(1), 93–112. https://www.idosr.org/wp-content/uploads/2021/07/IDOSR-JBESS-21-93-112-2017-1.pdf

[9] Onokwai, A. O., Okonkwo, U. C., Osueke, C. O., Ezugwu, C. A., Eze, N. C., Diarah, R. S., & Olawale, O. (2019). Quantifying cassava waste generation and biogas production in eHa-alumona grinding mills. International Journal of Civil Engineering and Technology, 10(1), 2032–2043.

[10] Salman, M., Bettany-Saltikov, J., Kandasamy, G., Whittaker, V., Hogg, J., & Racero, G. A. (2022). PROTOCOL: The effect of education programmes for improving knowledge of back health, ergonomics and postural behaviour in university students: A systematic review. Campbell Systematic Reviews, 18(1).

[11] Abasilim, C. F., Balogun, O. L., & Adeyemi, A. A. (2019). Analysis of the profitability and credit accessibility among Garri processors in Epe, Lagos State, Nigeria. Global Journal of Agricultural Sciences, 18(1), 57.

[12] Çetin, S., De Wolf, C., & Bocken, N. (2021). Circular digital built environment: An emerging framework. Sustainability (Switzerland), 13(11).

[13] Gervase Ikechukwu, A., & Paulina Chikaodili, I. (2020). Effects of Melon Seed or Soybean Meal Supplementation on the Physicochemical and Sensory Properties of Incompletely Peeled Cassava Garri. Journal of Food Technology Research, 7(1), 125–135.

[14] Ndife, J. (2019). Effect of palm oil inclusion on the quality of garri produced from white and yellow cassava (Manihot esculenta cranz) roots (Manihot esculenta cranz) roots. International Journal of Food Science and Nutrition, 4(3), 180–185.

[15] Nwadinobi, C., Edeh, J., & Mejeh, K. I. (2019). Design and Development of a Vertical Paddle Semi Automated Garri Frying Machine. Journal of Applied Sciences and Environmental Management, 23(7), 1279. https://doi.org/10.4314/jasem.v23i7.14
[16] Oloyede, T., Akintunde, A. A., Oloyede, T. W., Adeniran, J. A., Desalu, O. O., Tanimowo, M. O., & Salami, A. K. (n.d.). Air Quality Index and Respiratory Symptoms among Garri Processing Workers in Ogbomoso, Nigeria. West African Journal of Medicine, 37(2), 152–158. Retrieved April 4, 2022, from https://europepmc.org/article/med/32150634
[17] Onu, U. G. (2020). Design of Garri Frying Machine with User-defined Temperature Regulation and Motion Control System. International Journal for Research in Applied Science and Engineering Technology, 8(8), 1584–1589.
[18] Mohanty, B., & Hota, P. K. (2014). Particle swarm optimization based interconnected Hydro-Thermal AGC system considering GRC and TCPS. International Journal of Electrical and Computer Engineering, 8(7), 1195-1201.
[19] Abou Omar, M. S., Khedr, T. Y., & Abou Zalam, B. A. (2013, November). Particle swarm optimization of fuzzy supervisory controller for nonlinear position control system. In 2013 8th International Conference on Computer Engineering & Systems (ICCES) (pp. 138-145). IEEE.

[20] Samuel, A. U., Akinlabi, E. T., Okokpujie, I. P., & Fayomi, O. S. I. (2021). Sustainability of Garri Processing: A Case Study of Ogun State, Nigeria. IOP Conference Series: Materials Science and Engineering, 1107(1), 012132.
[21] Tsai, Y. T., Lee, C. H., Liu, T. Y., Chang, T. J., Wang, C. S., Pawar, S. J., Huang, P. H., & Huang, J. H. (2020). Utilization of a reinforcement learning algorithm for the accurate alignment of a robotic arm in a complete soft fabric shoe tongues automation process. Journal of Manufacturing Systems, 56, 501–513.